Journal of Biomedical Optics 6(4), 468–473 (October 2001)

Experimental verification of the effect of refractive index mismatch on the light fluence in a turbid medium

Thomas J. Farrell
Michael S. Patterson
Hamilton Regional Cancer and McMaster University
Ontario, Canada

Abstract. Diffusion theory is often used to model the transport of light within tissue. It can be used to calculate the light fluence rate in tissue, for example, during photodynamic therapy, or to measure the absorption and scattering properties of tissue. For both of these applications, the influence of the interface between the tissue and the exterior medium on the fluence rate inside the tissue must be known in order to make accurate calculations. We present an experimental investigation of the effect of the refractive index mismatch at the tissue interface on the internal light fluence rate and on the spatially resolved diffuse reflectance as the boundary conditions of the tissue/external medium are changed. The effects of changing the relative refractive index at the boundary are compared to predictions of diffusion theory. The effect of the refractive index mismatch is predicted correctly by diffusion theory. [DOI: 10.1117/1.1412222]

Keywords: tissue optics; diffusion theory; refractive index; photodynamic therapy.

Paper 20052 received Nov. 14, 2000; revised manuscript received Apr. 3, 2001; accepted for publication Apr. 12, 2001.

1 Introduction

Diffusion theory is often used to model the transport of light within tissue. This can be used to calculate the light fluence rate in tissue, for example, during photodynamic therapy,[1,2] and the accuracy of these calculations can be critical to success of the treatment. Other applications involve the measurement of diffusely reflected light which, combined with numerical optimization algorithms, can be used to infer bulk tissue optical properties, drug concentrations or in optical imaging.[3–8] In all of these applications the influence of the interface between the tissue and the exterior medium is important. Generally, when the refractive index of the tissue is different from that of the external medium, light will be internally reflected back into the tissue at the interface. This will change the internal fluence rate and will distort the spatial and temporal diffuse reflectance profiles. As a result, calculations of internal fluence rates for photodynamic therapy dosimetry or estimates of tissue optical properties based on reflectance are highly dependent on understanding the influence of the boundary conditions. In addition to this, understanding the effect of the boundary can be used to optimize photodynamic therapy, for example, by choosing whether to fill a balloon with a transparent or scattering liquid, or with air during photodynamic therapy of the bladder wall.[9]

The diffusion equation can be solved subject to boundary conditions at the interfaces.[10,11] These boundary conditions are derived by considering Fresnel's laws of reflection and balancing the fluence rate and photon current crossing the interface. There is a wealth of published data comparing Monte Carlo simulations to diffusion theory predictions, but to our knowledge there are few published data showing that the predicted influence of boundary conditions is actually realized in tissue. In a study by Marijnissen and Star[12] absolute fluence rate measurements were obtained in tissue and were compared with diffusion theory predictions. These predictions included both the influence of the boundary and the tissue optical properties, but did not separate them. We present an experimental investigation of the effect of the refractive index mismatch at the tissue interface on the light fluence rate inside the tissue as well as the spatially resolved diffuse reflectance. The effects are compared with those predicted by diffusion theory.

2 Materials and Methods

Two complementary experiments were performed. The first experiment investigated the effect of the boundary conditions on the internal fluence rate from an externally applied broad-beam light source. The second experiment investigated the effect of boundary conditions on the steady-state reflectance of a pencil beam from the medium.

2.1 Internal Fluence Rate

This experiment was performed in transmission geometry (see Figure 1). A gel phantom was placed inside a transparent glass container and broad-beam light (with a beam diameter greater than the area of the container) entered the phantom through the bottom of the container. The relative refractive index at the upper surface of the phantom was adjusted by introducing a transparent liquid layer above the phantom. This arrangement maintained a constant refractive index at the entrance surface of the phantom so that the total power entering the phantom was not perturbed by refractive index changes at the boundary. The gel phantom was easily liquefied upon heating, and it was therefore possible to place optical fibers at arbitrary

Address all correspondence to Thomas J. Farrell. Tel: 1 905-387-9495; Fax: 1 905-575-6330; E-mail: tom.farrell@hrcc.on.ca

1083-3668/2001/$15.00 © 2001 SPIE

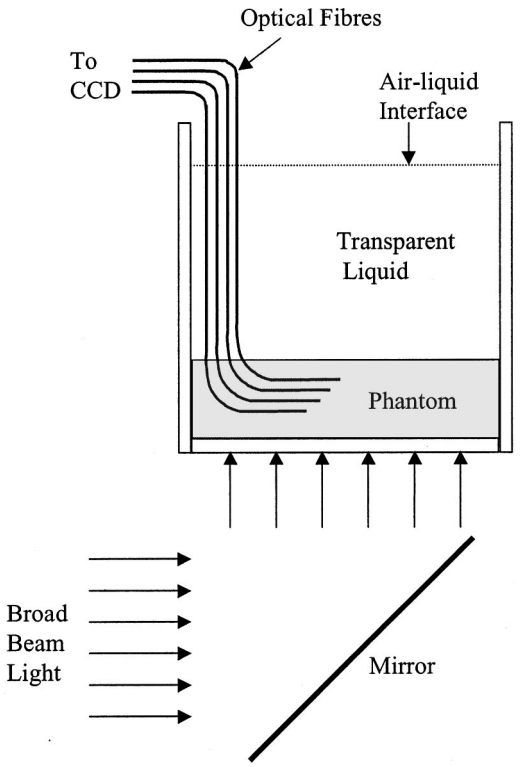

Fig. 1 Schematic diagram of configuration used for internal fluence measurements in transmission geometry. Broad-beam light enters through transparent bottom of container, and four optical fibers measure the internal fluence at different depths in the phantom as the depth of the transparent liquid above the phantom is changed.

locations inside the phantom before re-solidifying the phantom. The light source was a halogen bulb housed within a slide projector. The relative light fluence rate was measured via the four embedded optical fibers while a reference fiber was placed in the incident beam to monitor fluctuations in source output. These were coupled to a charge coupled device (CCD) based spectrometer which allowed measurements of the spectral fluence rate at all four depths. The embedded fibers had cut ends and were oriented perpendicular to the incident light source in order to make them insensitive to the unscattered primary light. The minimum depth of the detection fibers was 10 mm and at this depth and beyond there is no depth dependence to the directional dependence of the radiance.

The phantom consisted of ethylene glycol, with gelatin as a thickening agent and titanium oxide as a light-scattering agent. The total thickness of the phantom was 22 mm and the optical properties of the phantom were measured using both steady-state[13] and time resolved reflectance.[14] The transport scatter coefficient was 0.63 mm^{-1} and the absorption coefficient was 0.003 mm^{-1} at 650 nm and the refractive index was 1.47. The two transparent liquids were water, $n=1.33$, and phenoxyethanol, $n=1.54$. Four fibers were spaced at nominal depths of 1, 5, 7.5 and 10 mm from the top of the phantom. The true fiber depth was determined by slicing the phantom vertically through the level of the fibers and measuring the depth from the surface.

This experiment was repeated using whole chicken breast with the following small changes in protocol. The optical fibers were introduced via 17 gauge needles, which were removed (leaving the fibers in place) for the fluence rate measurements. Olive oil was chosen as the liquid above the tissue because both water and phenoxyethanol degraded the tissue surface and changed the internal reflection over time.

Optical diffusion theory was used to calculate the internal light fluence rate under the experimental conditions. The steady-state diffusion equation for this geometry is

$$\frac{d^2\Phi(z)}{dz^2}-\mu_{\text{eff}}^2\Phi(z)=-\frac{P\mu_s'}{D}\exp[-\mu_t',z], \tag{1}$$

where $\Phi(z)$ is the internal diffuse fluence rate as a function of depth, z, $D=1/3\mu_t'$ is the diffusion coefficient, $\mu_t'=\mu_a+\mu_s'$ is the transport coefficient, $\mu_{\text{eff}}=\sqrt{(\mu_a/D)}$ is the effective attenuation coefficient, $\mu_s'=\mu_s(1-g)$ is the transport scattering coefficient, and μ_s, μ_a, and g are the scatter and absorption coefficients and the anisotropy parameter (mean cosine of scattering angle), respectively. The right-hand side includes the diffuse photon source term which is approximated as the depth dependent ''first'' isotropic scatter probability. This is given as the product of μ_s' and the attenuated primary fluence rate $P\exp[-\mu_t' z]$ where P is the incident fluence rate. The depth is set to zero on the entrance surface and increases towards the top surface.

The boundary conditions at the interfaces are obtained by setting the irradiance at the boundary equal to the integral of the reflected radiance[10] and can be expressed in the following form:

$$\begin{aligned} 2A_E D\frac{d\Phi(z)}{dz}&=\Phi(z)[\text{Entrance}];\\ 2A_T D\frac{d\Phi(z)}{dz}&=-\Phi(z)\ \ [\text{Top surface}], \end{aligned} \tag{2}$$

where $A=(1+R_{\text{eff}})/(1-R_{\text{eff}})$, and R_{eff} is the effective reflection coefficient, which can be found by integrating the Fresnel reflection coefficient over all incident angles.[10] For the gel phantom $A_E=3.415$, and $A_T=3.415$, 1.370 and 1.020 for air, water and phenoxyethanol above the phantom. If we assume a value for the refractive index of tissue of 1.4,[15] then the calculated values for the chicken breast are $A_E=2.945$ and $A_T=2.945$ for air and 1.167 for olive oil. The internal fluence rate is given as

$$\Phi(z)=G_1e^{-\mu_{\text{eff}}z}+G_2e^{\mu_{\text{eff}}z}+G_3e^{-\mu_t' z}, \tag{3}$$

where $G_e=-\mu_S'P/D(\mu_t'^2-\mu_{\text{eff}}^2)$ and G_1 and G_2 can be found by solving the following equation:

$$\begin{pmatrix} (\mu_{\text{eff}}2A_TD-1)e^{-\mu_{\text{eff}}z} & -(\mu_{\text{eff}}2A_TD+1)e^{\mu_{\text{eff}}z} \\ -(1+\mu_{\text{eff}}2A_ED) & (\mu_{\text{eff}}2A_ED-1) \end{pmatrix}\begin{pmatrix} G_1 \\ G_2 \end{pmatrix} = \begin{pmatrix} (1-\mu_t'2A_TD)e^{-\mu_t' z} \\ 1+\mu_t'2A_ED \end{pmatrix} G_3. \tag{4}$$

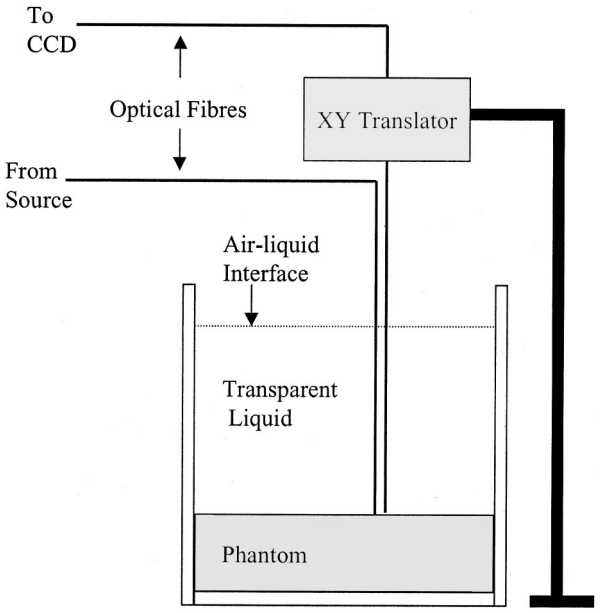

Fig. 2 Schematic diagram of configuration used for reflectance measurements. A pencil beam of light enters the phantom from the source optical fiber and the spatially resolved reflectance is measured by changing the separation between the source and detector fibers as the depth of the transparent liquid above the phantom is changed.

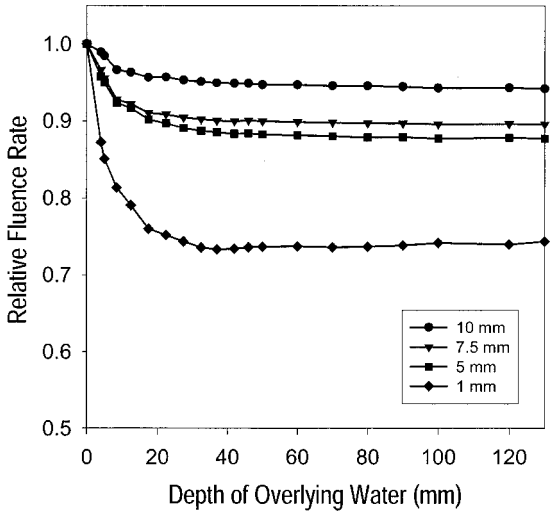

Fig. 3 Relative internal fluence rate as a function of depth of overlying liquid at four depths in the phantom. Fluence rate at each measurement position is normalized to the fluence rate at overlying layer depth=0. Phantom optical properties at 633 nm are $\mu_s' = 0.63$ and $\mu_a = 0.003$ mm^{-1}. At depths of overlying water greater than 40 mm the relative fluence is constant and is equal to that for a semi-infinite layer of water above the phantom.

2.2 Steady-State Reflectance

The second experiment was performed in reflection geometry (see Figure 2). A pencil beam of light was introduced into a phantom using a 400 μm core optical fiber held directly in contact with the upper surface of the phantom. A second 400 μm core detection fiber was held less than 0.5 mm above the phantom to collect the diffusely reflected light. This was mounted on an *XY* translation stage which allowed accurate adjustment of the distance between the two fibers. The detection fiber was coupled to the spectrometer as before. The phantom was prepared using TiO_2 in a solid polystyrene ($n = 1.59$) matrix.[16] This was used, rather than the gel phantom, so that the upper surface could be machined to produce a smooth flat interface with the liquid. The relative refractive index at the upper surface was adjusted by introducing water above the phantom. Because the collection fiber was held above the phantom, the collection aperture was different when the upper layer was air or water. We have run Monte Carlo simulations (not included) that show virtually no radial dependence in the directional response of the detection fibers for radial distances greater than 1 mm. Thus, the difference in collection aperture affected the absolute response of the detection system but not the relative radial response.

As above, optical diffusion theory was used to calculate the diffuse reflectance rate under the experimental conditions. The steady-state diffusion equation for this geometry is given as

$$\nabla^2 \Phi(\mathbf{r}) - \mu_{\text{eff}}^2 \Phi(\mathbf{r}) = -\frac{S(\mathbf{r})}{D}. \tag{5}$$

The boundary condition at the entrance surface was given by Eq. (2). The expression for the reflectance derived by Kienle and Patterson[11] using diffusion theory was used. Briefly, the source term was modeled as a point scattering source at a depth of one mean free path, $z_0 = 1/\mu_t'$, and the extrapolated boundary approach was used to satisfy the boundary condition. The spatially resolved steady-state reflectance per incident photon, $R(\rho)$, was calculated using

$$R(\rho) = \frac{F_R}{4\pi}\left\{ z_0\left(\mu_{\text{eff}} + \frac{1}{r_1}\right)\frac{\exp^{-\mu_{\text{eff}} r_1}}{r_l^2} + (z_0 + 2z_b)\left(\mu_{\text{eff}} + \frac{1}{r_2}\right)\frac{\exp^{-\mu_{\text{eff}} r_2}}{r_2^2}\right\} + \frac{F_\Phi}{4\pi D}\left\{\frac{\exp^{-\mu_{\text{eff}} r_1}}{r_1} - \frac{\exp^{-\mu_{\text{eff}} r_2}}{r_2}\right\}, \tag{6}$$

where $r_1 \sqrt{z_0^2 + \rho^2}$; $r_2 = \sqrt{(z_0 + 2z_b)^2 + \rho^2}$ and $z_b = 2AD$ is the distance to the extrapolated boundary. The parameters F_R and F_Φ represent the fractions of the fluence rate and the flux which exit the tissue across the interface. These values are obtained by integration of the radiance over the backward hemisphere.[11] For the polystyrene phantom the values F_R and F_Φ were 0.089 and 0.239 for air, and 0.169 and 0.406 for water above the phantom. Expression (6) was used to fit the measured reflectance data in order to derive the scatter and absorption coefficients of the phantom.

3 Results

3.1 Internal Fluence Rate

In order to assess the effect of internal reflection at the top of the overlying liquid layer, the light signal at each optical fiber was measured as the depth of the liquid was increased. Results are shown in Figure 3 where water was the transparent liquid. The general trend for all four detection fibers is that

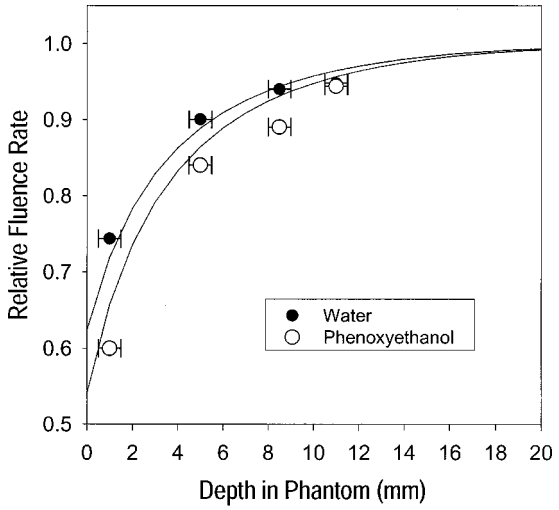

Fig. 4 Relative internal fluence of liquid/phantom to air/phantom interface at four depths in the phantom. The different symbols represent different transparent liquids and the solid curves correspond to diffusion theory calculations using the experimental optical properties and refractive index changes. Phantom optical properties are as in Figure 3.

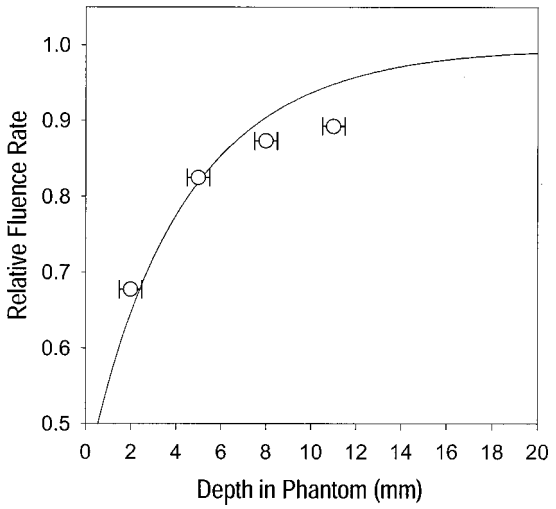

Fig. 5 Similar to Figure 4. Relative internal fluence of olive oil/tissue to air/tissue interface at four depths in the phantom. Solid curve is diffusion theory calculation using published optical properties for chicken breast muscle.

measured light fluence rate decreased relative to the initial value (phantom/air interface depth=0), and near a depth of 40 mm a constant relative fluence rate was achieved. Beyond this depth, there is no influence of internal reflection at the water/air boundary and the measured relative fluence rate is equal to that for a semi-infinite layer of water above the phantom. A similar set of measurements (not shown) was performed using phenoxyethanol.

The relative fluence rate (phantom/liquid to phantom/air) was determined for both water and phenoxyethanol at all four depths in the phantom with more than 40 mm overlying liquid (see Figure 4). The greatest source of uncertainty in the measured data was the measurement of the depth of the fibers and is shown as a horizontal error bar. Adding the transparent liquid changed the relative refractive index at the interface from 1.47 to 1.10 (water) or 0.95 (phenoxyethanol). This resulted in a reduction in the amount of light internally reflected back into the phantom from the upper surface and hence reduced the internal fluence rate. This effect was greatest near the upper surface, where the ratio of forward/backward propagating light is the least. The difference was also greater for phenoxyethanol because it introduces a larger change in reflectance than water.

The diffusion theory expression [Eq. (3)] was used to calculate the relative fluence rate (phantom/liquid to phantom/air) for both water and phenoxyethanol at all depths in the phantom. These results are plotted as solid curves in Figure 4. Overall, the measured effect of changing the refractive index mismatch is modeled well by theory.

The experiment was repeated using chicken breast and olive oil and the results are plotted in Figure 5. The reduction in relative fluence rate is similar to that seen with the gel phantom. The solid curve represents the diffusion theory calculations and is based on published values for the tissue index of refraction[15] $n=1.4$, and optical properties[17] $\mu_s'=0.33$ and $\mu_a=0.017\ \text{mm}^{-1}$. At shallow depths the theoretical model predicts well the effect of the interface, but is less accurate at greater depths.

3.2 Steady-State Reflectance

The spatially resolved reflectance for different depths of water overlying the phantom is shown in Figure 6. In this graph $\ln[\rho^2 R(\rho)]$ is plotted against ρ, where ρ is the radial distance and $R(\rho)$ is the measured diffusely reflected light normalized to the value at $\rho=1.1$ mm. As the water depth changed, the

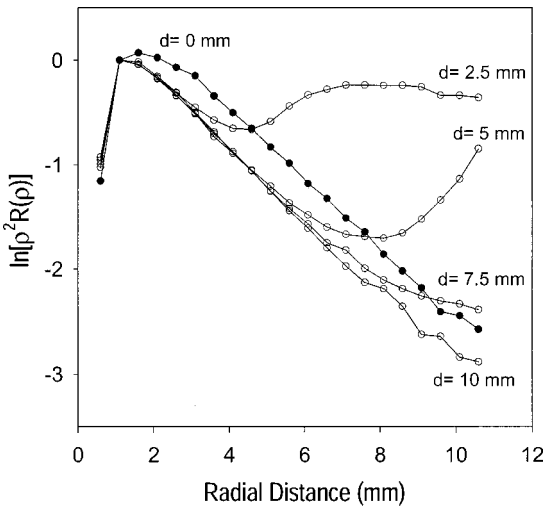

Fig. 6 Spatially resolved reflectance from polystyrene phantom with different depths of water overlying the phantom. The solid circles are for an air/phantom interface ($d=0$ mm) and the open circles are for different depths of water above phantom. The log of the reflectance multiplied by the square of the radial distance is plotted. Note the presence of a depth dependent artifact for all depths greater than 0 mm due to internal reflectance at the water/air boundary. For water depths greater than 7.5 mm the artifact does not affect the reflectance over the range of radial distances presented and the reflectance is equal to that for a semi-infinite layer of water overlying the phantom.

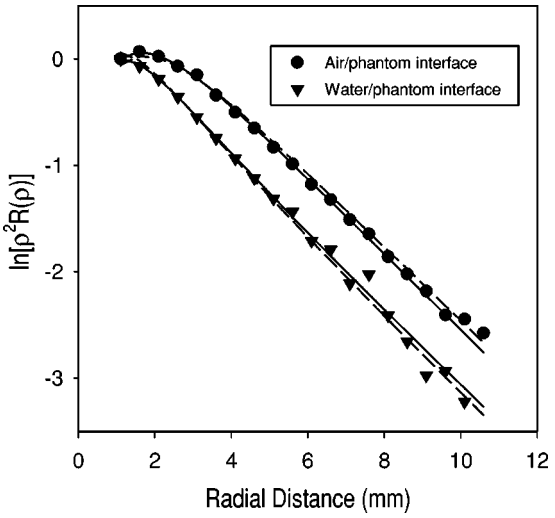

Fig. 7 Spatially resolved reflectance from polystyrene phantom with air/phantom and water/phantom interfaces. As in Figure 6, the log of the reflectance multiplied by the square of the radial distance is plotted. The symbols are the measured data, the solid curves are least squares fits of the data to the diffusion theory model [Eq. (6)], and the dashed curves are forward calculations of Eq. (6) using the means of the fitted optical properties for the two different interfaces.

reflectance curve changed from its initial shape at $d=0$, corresponding to a relative refractive index mismatch, n_{rel}, of 1.59 at the surface, to its final form at $d=10$ mm, with $n_{\text{rel}}=1.2$.

The curves at the intermediate depths show an interesting artifact. There is a secondary minimum in the curve and the reflectance is elevated beyond this. This artifact is due to light which has been diffusely reflected from the phantom from extremely short distances, then has been internally reflected from the water/air interface back into the phantom and is then diffusely reflected again. It appears as a ring of light in a two-dimensional view. This effect has been observed and explained by other investigators when illuminating a diffuse reflecting surface on a glass plate.[18] The magnitude and location of this structure is highly dependent on the thickness of the overlaying water layer, but at a depth of 10 mm it appears beyond a radius of 10 mm (not shown) and does not affect the reflectance curve at closer distances. At this depth, the reflectance curve can be considered equivalent to that with a semi-infinite volume of water above the phantom.

If the curves for depth 0 mm (air/phantom interface) and depth 10 mm (water/phantom interface) are compared, two phenomena can be noted. First, at large distances, the slopes of these curves are similar (in fact the slope approaches μ_{eff}). Second, the radial distance of the peak is greater for the air/phantom interface. This is due to light which has been internally reflected at the interface at a short distance escaping at a larger distance.

The spatially resolved reflectance for water and air above the phantom was fitted to Eq. (6) using the Marquardt least squares fitting algorithm[19] and the results are shown as solid curves in Figure 7. The fitted curves match the measured data. The fitted optical properties were $\mu_s'=2.64$ and $\mu_a=0.0150\ \text{mm}^{-1}$ for air, and $\mu_s'=2.32$ and $\mu_a=0.0157\ \text{mm}^{-1}$ for water over the phantom. The fitted values for the different boundary conditions agree to within 13% and 5% for the scatter and absorption coefficients, respectively. Published reports[4] suggest that the accuracy of optical property estimates using steady-state reflectance is of the order of 5%–10%. Within this uncertainty level, the fitted values are not affected by changes in the boundary conditions. To further understand the effect, the average of the fitted optical properties was used to calculate the reflectance using both the water and air boundary conditions. These are plotted in Figure 7 using dashed lines. These curves match the data well except at the very short distances where diffusion theory may no longer be valid.

4 Discussion and Conclusions

This investigation was undertaken to verify the influence of the boundary conditions on the diffuse internal fluence rate and diffuse reflectance predicted by diffusion theory. The relative refractive index at the surface of a phantom or a tissue sample was changed by adding a layer of transparent liquid above it. The changes in the internal fluence rate or reflectance relative to the initial phantom/air interface were compared with predicted changes.

Adding the transparent liquid above the phantom caused the internal fluence rate to decrease relative to the air/phantom interface. This is due to reduced internal reflection back into the phantom from the interface. The magnitude of the effect is modeled well by diffusion theory. The same effect was seen when the experiment was repeated using the tissue sample. The results indicate that the predicted effect of the boundary conditions is observed both in phantoms and in real tissue samples.

Adding the transparent liquid above the phantom caused the spatially dependent diffuse reflectance curve to change shape. The final slope of the curves was the same, but the peak position moved to larger distances. When the reflectance was fitted using the diffusion model, the optical properties obtained from the best fit lines were within 13% of each other. The curves calculated using the average best fit matched the data well except at short distances.

Both of these results were obtained under conditions (large depth, large radial distance) where the fluence is well described by diffusion theory. At very shallow depths where the incident light contributes to the fluence and at small radial distances where singly scattered photons contribute to the reflectance, the radiance will be highly anisotropic and the internal reflection at the surface will not be described by the boundary condition given in Eq. (2). In these regions diffusion theory will not adequately describe the fluence and more complicated transport models are needed.

Under conditions where diffusion theory can be used to model light transport in tissue, the influence of the boundary conditions on diffuse internal fluence rate and diffuse reflectance are predicted well both phenomenologically and quantitatively by diffusion theory.

Acknowledgments

The authors would like to thank the National Cancer Institute of Canada and the National Institutes of Health (PO1-CA43892) for financial support. Assistance with the experi-

mental work provided by Jody Bruulsema, Phil Eles, Andy Ayeung and Catriona Syme is also appreciated.

References

1. W. M. Star, B. C. Wilson, and M. S. Patterson, ''Light delivery and optical dosimetry in photodynamic therapy of solid tumors,'' in *Photodynamic Therapy*, B. W. Henderson and T. J. Dougherty, Eds., pp. 335–368, Dekker, New York (1992).
2. B. J. Tromberg, L. O. Svaasand, M. K. Fehr, S. J. Madsen, P. Wyss, B. Sansone, and Y. Tadir, ''A mathematical model for light dosimetry in photodynamic destruction of human endometrium,'' *Phys. Med. Biol.* **41**, 233–237 (1996).
3. R. A. Weersink, J. E. Hayward, K. R. Diamond, and M. S. Patterson, ''Non-invasive *in vivo* measurements of photosensitizer uptake using diffuse reflectance spectroscopy,'' *Photochem. Photobiol.* **66**, 326–335 (1997).
4. M. G. Nichols, E. L. Hull, and T. H. Foster, ''Design and testing of a white-light steady-state diffuse reflectance spectrometer for determination of optical properties of highly scattering systems,'' *Appl. Opt.* **36**, 93–104 (1997).
5. S. J. Madsen, E. R. Anderson, R. C. Haskell, and B. J. Tromberg, ''Portable high-bandwidth frequency-domain photon migration instrument for tissue spectroscopy,'' *Opt. Lett.* **19**, 1934–1936 (1994).
6. S. Fantini, M. Franceschini, S. Fishkin, B. Barbieri, and E. Gratton, ''Quantitative determination of the absorption spectra of chromophores in strongly scattering media: A light-emitting diode-based technique,'' *Appl. Opt.* **33**, 5204–5213 (1994).
7. M. Fabiani, G. Gratton, and P. M. Corballis, ''Noninvasive near infrared optical imaging of human brain function with subsecond temporal resolution,'' *J. Biomed. Opt.* **1**, 387–398 (1996).
8. H. Jiang, K. D. Paulsen, U. L. Osterberg, and M. S. Patterson, ''Frequency-domain near-infrared photo diffusion imaging: Initial evaluation in multitarget tissuelike phantoms,'' *Med. Phys.* **25**, 183–193 (1998).
9. H. J. Van Staveren, M. Keijzer, T. Keesmaat, H. Jansen, W. J. Kirkel, J. F. Beek, and W. M. Star, ''Integrating sphere effect in whole-bladder wall photodynamic therapy: III. Fluence multiplication, optical penetration and light distribution with an eccentric source for human bladder optical properties,'' *Phys. Med. Biol.* **41**, 579–590 (1996).
10. R. C. Haskell, L. O. Svaasand, T. T. Tsay, T. C. Feng, M. N. McAdams, and B. J. Tromberg, ''Boundary conditions for the diffusion equation in radiative transfer,'' *J. Opt Soc. Am. A* **11**, 2727–2741 (1994).
11. A. Kienle and M. S. Patterson, ''Improved solutions of the steady-state and time-resolved diffusion equations for reflectance from a semi-infinite turbid medium,'' *J. Opt. Soc. Am. A* **14**, 246–254 (1997).
12. J. P. A. Marijnissen and W. M. Star, ''Quantitative light dosimetry in vitro and in vivo,'' *Lasers Med. Sci.* **2**, 235–241 (1987).
13. J. T. Bruulsema, J. E. Hayward, T. J. Farrell, M. S. Patterson, L. Heinemann, M. Berger, K. Koschinsky, J. Sandahl-Christiansen, H. Orskov, M. Essenpreis, G. Schmelzeisen-Redeker, and D. Boecker, ''Correlation between blood glucose concentration in diabetics and noninvasively measured tissue optical scattering coefficient,'' *Opt. Lett.* **22**, 190–192 (1997).
14. R. Hunter, ''Measuring hemoglobin oxygenation by time resolved reflectance,'' MSc thesis, McMaster University (1998).
15. F. P. Bolin, L. E. Preuss, R. C. Taylor, and R. J. Ference, ''Refractive index of some mammalian tissues using a fiber optic cladding method,'' *Appl. Opt.* **28**, 2297–2303 (1989).
16. T. J. Farrell, R. P. Hawkes, M. S. Patterson, and B. C. Wilson, ''Modeling of photosensitizer fluorescence emission and photobleaching for photodynamic therapy dosimetry,'' *Appl. Opt.* **37**, 7168–7183 (1998).
17. W. Cheong, S. A. Prahl, and A. J. Welch, ''A review of the optical properties of biological tissues,'' *IEEE J. Quantum Electron.* **26**, 2166–2185 (1990).
18. M. Bourdinaud and H. Blumenfeld, ''Rings observed on a transparent plate coated with a diffusing layer,'' *Appl. Opt.* **26**, 4009–4013 (1987).
19. P. R. Bevington, *Data reduction and error analysis for the physical sciences*, McGraw–Hill, New York (1969).